Applied Catalysis B: Environmental 236 (2018) 25–35

Contents lists available at ScienceDirect

Applied Catalysis B: Environmental

journal homepage: www.elsevier.com/locate/apcatb

Cu_x-$Nb_{1.1-x}$ (x = 0.45, 0.35, 0.25, 0.15) bimetal oxides catalysts for the low temperature selective catalytic reduction of NO with NH_3

Sher Ali, Liqiang Chen, Zhibin Li, Tianrui Zhang, Rui Li, Syed ul Hasnain Bakhtiar, Xuesong Leng, Fulong Yuan, Xiaoyu Niu*, Yujun Zhu*

Key Laboratory of Functional Inorganic Material Chemistry (Heilongjiang University), Ministry of Education, School of Chemistry and Materials, Heilongjiang University, Harbin, 150080, PR China

ARTICLE INFO

Keywords:
Cu and Nb bimetal oxides
Selective catalytic reduction
NO removal
Synergistic effect

ABSTRACT

The Cu_x-$Nb_{1.1-x}$ (x = 0.45, 0.35, 0.25, 0.15) bimetal oxides catalysts were synthesized through citric acid method and used in the selective catalytic reduction (SCR) of NO with NH_3. The relationship among the catalytic performances, the acid/redox properties and the structures of the binary oxides systems was explored through different characterization techniques including XRD, H_2-TPR, BET, NO-TPD, NH_3-TPD, XPS and in situ DRIFTS. The characterization results point out that the ratio of Cu to Nb has great influence on the activity of NH_3-SCR reaction. Different catalytic activities of Cu_x-$Nb_{1.1-x}$ (x = 0.45, 0.35, 0.25, 0.15) mixed oxides could be attributed mainly to surface area, acid amount, the adsorption and activation of NH_3 and redox ability of the corresponding catalyst. Among these Cu_x-$Nb_{1.1-x}$ (x = 0.45, 0.35, 0.25, 0.15) oxides catalysts, the $Cu_{0.25}$-$Nb_{0.85}$ catalyst exhibited the complete NO conversion in a reaction temperature range of 180-330 °C, together with near 100% N_2 selectivity and remarkable SO_2/H_2O resistance. Moreover, the $Cu_{0.25}$-$Nb_{0.85}$ catalyst still exhibited wide activity temperature window of 185-380 °C at above 90% NO conversion even in the presence of 5% H_2O under high GHSV of 70,000 h^{-1}. Thus, it can be summarized from the above results that $Cu_{0.25}$-$Nb_{0.85}$ can be considered as excellent catalyst for NH_3-SCR of NO.

1. Introduction

The abatement of atmospheric pollution is a challenging task worldwide. It becomes more and more severe with passage of time, and therefore large number of people have been involved in environmental protection awareness. Among the atmospheric pollutants, NO_x (nitrogen oxides) is one of main contributor, which is responsible for ozone depletion, acid deposition photochemical smog and greenhouse effect [1–4]. NO_x is mainly emitted from mobile resources such as diesel engines and stationary resources like coal-fired power plants etc. [1–4]. NO_x can be abated through different de-nitrification techniques such as adsorption method, pulse corona plasma, electron beam irradiation, selective non-catalytic reduction and selective catalytic reduction (SCR) of NO_x with NH_3 (NH_3-SCR) [3–5]. Among these denitrification techniques, the NH_3-SCR has been considered as the most successful, encouraging, interesting, imperative and commercial employed procedure for NO_x abatement from stationary boilers and coal-fired plants [6–10]. Commercially, the V_2O_5-$WO_3(MoO_3)$-TiO_2 catalyst has been extensively employed for NO_x reduction in electric plant owing to its outstanding catalytic activity [6,9,11]. Nevertheless, there are still some shortcomings, which constrain their usage for nonelectric plant such as the biological toxicity of V_2O_5 to human being and eco-environment, narrow NH_3-SCR reaction range of (300-400 °C), and unselective oxidation of NH_3 to produce N_2O at high temperature [12–14]. Furthermore, the temperature of exhaust smoke NO_x emitted from stationary resources such as industrial boiler, coal-fired power plants, coker heater, combustion furnaces, industrial boiler and glass melting stove, is lower than 300 °C in general [15,16]. The conventional V_2O_5-$WO_3(MoO_3)$-TiO_2 catalyst is not effective for above exhaust smoke NO_x. Therefore, it is compulsory to develop environmental-friendly NH_3-SCR catalysts with exceptional low-temperature NO conversion, high N_2 selectivity and a broad operating temperature window as alternatives.

In the last decade, numerous transitional metal oxides such as MnO_x, CeO_2, FeO_x, NiO, CuO_x and large number of mixed metal oxides, have been reported and attracted great attention due to its fascinating low-temperature NH_3-SCR of NO activity [11,17–19]. MnO*x* and other manganese-containing catalysts presented fascinating low-temperature NH_3-SCR of NO activity [10]. However, it is important for low temperature application to improve N_2 selectivity, the poisoning resistance to H_2O and sulfur oxides. On the other hand, the commonly reported Cu

* Corresponding authors.
E-mail addresses: niuxiaoyu@hlju.edu.cn (X. Niu), yujunzhu@hlju.edu.cn (Y. Zhu).

https://doi.org/10.1016/j.apcatb.2018.05.014
Received 17 January 2018; Received in revised form 25 April 2018; Accepted 6 May 2018
Available online 06 May 2018
0926-3373/

containing catalysts such as Cu/SAPO-34 (Cu exchanged zeolites), which exhibited superior low temperature NH_3-SCR activity [20]. However, owing to high price of Cu/SAPO-34 [20] and Cu-SSZ-13 [21], the mixed metal oxides of Cu and others transitional metals were developed for NH_3-SCR of NO reaction at lower temperature. Si et al. [19] prepared the impregnated CuO_x on the WO_3-ZrO_2 support, the resultant catalyst showed good NH_3 adsorption, and fascinating low-temperature NH_3-SCR of NO activity in range of 200-320 ˚C. The CuO is widely used as active species in different catalytic processes [22–24]. Sullivan et al. [25], described that the Cu mixed metal oxides prepared from two different metal salts ($CuSO_4$ and $Cu(NO_3)_2$) supported on different oxides (TiO_2, Al_2O_3 and SiO_2) showed exceptional NH_3-SCR activity in a broad temperature window. According to Guo et al. study [26], the Cu and Ce mixed metal oxide catalyst (CuO-CeO_2) exhibit fascinating low-temperature NH_3-SCR of NO activity, and it was also pointed out that the oxidation state of Cu on the catalyst surface effect the NH_3-SCR activity. The ternary metal oxides of Cu, Ce and Ti (Ce-Cu-Ti) exhibited excellent NH_3-SCR activity even in the presence of H_2O and SO_2 [30]. Many other researchers also reported that $CuO/WO_3/Ce_{0.5}Zr_{0.5}O_2$, $CuO/CeO_2/ZrO_2$, and $CuO\text{-}CoO_x/Ce_{0.67}Zr_{0.33}O_2$ demonstrated outstanding NO_x conversion in a wide temperature window of 220-450 ˚C [22–24]. In our previous work [27], it was found that $Cu_{0.2}$-$Ce_{0.3}$-$Zr_{0.5}$ oxides displayed especial NH_3-SCR activity, 100% N_2 selectivity in a temperature window of 150-270 ˚C, and maintained this performance even in the presence of H_2O/SO_2 and high gas hourly space velocity (GHSV) of 84,000 h^{-1}. However, the activity window was not enough wide (only 120 ˚C). Thus, it is still a challenge to prepare Cu-based catalysts having outstanding NH_3-SCR activity at low temperature with wide activity window and much better H_2O and SO_2 resistance.

In addition, the Nb-containing compounds such as Nb_2O_5/FeOx [28], V_2O_5-Nb_2O_5/TiO_2 [29], and Ag-Nb_2O_5/Al_2O_3 [30] were synthesized and were used in NH_3-SCR activity for removal of NO_x due to strong acidity of niobium oxides. The addition of Nb can noticeably improve the NH_3-SCR reactivity and decrease the unselective NH_3 oxidation at high temperatures over MnOx-CeO_2 catalyst [31]. Furthermore, the catalytic active sites were remarkably increased due to strong interaction between Nb and Mn. Qu et al. reported that the CeO_2-Nb_2O_5 catalyst exhibited excellent NH_3-SCR activity because of the abundant surface absorbed oxygen [32]. Consequently, Nb may be an excellent choice to enhance the low-temperature NH_3-SCR activity and SO_2/H_2O resistance for Cu-based catalysts. Moreover, the information such as the structure-activity relationship and the active sites are very important for the excellent NH_3-SCR of NO_x activity. The relationships among the catalytic activity, the acid/redox properties and the structures of the binary systems are seldom investigated.

In the present work, a series of Cu_x-$Nb_{1.1-x}$ (x = 0.45, 0.35, 0.25, 0.15) oxides catalysts were synthesized by a citric acid method and were used in the NH_3-SCR of NO process. The synthesized Cu_x-$Nb_{1.1-x}$ catalysts displayed outstanding SCR activity, N_2 selectivity and SO_2/H_2O resistance. Various characterization methods such as Raman, XRD, TEM, H_2-TPR, NO-TPD, NH_3-TPD, XPS and in situ DRIFTS were used to explore the structure, redox ability and reactivity of adsorbed NO_x and NH_3 species on the catalysts. The characterization results reveal that the surface area, redox ability and reactivity of NH_3 together with absorbed nitrate are notably enhanced for the binary Cu and Nb oxides.

2. Experimental

2.1. Catalyst preparation

Through citric acid method, Cu_x-$Nb_{1.1-x}$ (x = 0.45, 0.35, 0.25, 0.15) bimetal oxides catalysts were synthesized. Briefly, the designated ratios of copper nitrate (0.45-0.15 mol) and niobium (V) chloride (0.95-0.65 mol) were mixed. First, the niobium (V) chloride was dissolved in 50 mL ethanol, and copper nitrate was dissolved in aqueous citric acid (0.05 mol/50mL), then both the solution were mixed together and stirred for 5 h. Then, the solution was dried for 10 h at 140 ˚C and consequently porous foam like solid materials were obtained. These foam materials were crushed and were calcined at 500 ˚C for 5.0 h in air in muffle furnace. The resultant samples were finally crushed and sieved to 40-60 mesh for testing the catalytic activity. According to the above method, the CuO and Nb_2O_5 as references were also prepared.

2.2. Characterizations

Through Micromeritics TristarII 3020 instrument, the specific BET surface area was recorded in liquid N_2 temperature (-196 ˚C). Before BET experiment, the desired catalysts were degassed for 8 h at 150 ˚C under vacuum. The Bruker D8 Advance using a Cu Kα (λ =1.5418Å) radiation source (40 kV, 40 mA) was used for powder X-ray diffraction (XRD) data was collection. The X-ray diffraction data were recorded with 0.02 ˚ intervals in the *2θ* range of 5-80 ˚. The Kratos-AXIS ULTRA DLD instrument equipped with a monochromatic Al Kα X-ray source was used for X-ray photoelectron spectra (XPS) measurement. The internal binding energy (BE) was standardized using the carbon deposit C1s BE of 284.4 eV. The elemental analysis was carried out through X-ray fluorescence spectrometer (XRF) on a Bruker S4 Explorer instrument. Transmission electron microscopy (TEM) experiments were performed by using an FEI Tecnai G2 with an accelerating voltage of 200 kV.

The Tianjin XQ TP5080 auto adsorption device was used for investigating the temperature-programmed reduction by hydrogen (H_2-TPR) properties of the samples. Typically, 0.020 g sample was pretreated for 1 h at 300 ˚C in a flow of pure O_2 (25 mL·min^{-1}), and then cooled down to room temperature. In the next step, the 5% H_2/N_2 gas was switched on and the sample was heated from 30 ˚C to 900 ˚C with heating rate of 10 ˚C·min^{-1}. Thermal conductivity detector (TCD) was used for recording H_2 consumption.

The NH_3/NO temperature-programmed desorption (NH_3-TPD / NO-TPD) experiments were conducted through Tianjin XQ TP5080 auto-adsorption instrument. The instrument was equipped with thermal conductivity detector (TCD). In the first step, 100 mg of catalyst was pretreated for 1 h at 300 ˚C in presence of He flow (30mL·min^{-1}), and cooled to 25 ˚C under the same He flow. In the second step, pure NH_3/NO (25 mL·min^{-1}) was passed from the sample at 25 ˚C for 30 min, and followed by purging with He (30mL·min^{-1}) for 1 h. In the third step, the sample was heated from 25 ˚C to 700 ˚C at a rate of 10 ˚C·min^{-1} in He (30 mL·min^{-1}) and the corresponding TPD curve was recorded. In NO-TPD experiment, mass spectra (QIC-20, Hidden) was also used to detect the signals of N_2 (m/z=28), N_2O (m/z = 44), O_2 (m/z =32) or NO_2 (m/z =46).

The *in-situ* DRIFTS study was carried out through FTIR spectrometer (Nicolet 6700) equipped with a DRIFTS cell (Harrick) and a highly sensitive MCT detector cooled by liquid N_2. The spectra were recorded with 64 co-added scans of 4 cm^{-1} resolution. The background spectrum was collected in the presence of N_2 flow. Initially, N_2 (200 mL·min^{-1}) gas was passed from the sample at 360 ˚C for 1 h in order to clean the sample from impurities, and in the same gas flow the sample was cooled to chosen temperature. In the next step, 1000 ppm NO (when used), 1000 ppm NH_3 (when used) and 3 vol% O_2 (when used) were passed from the sample, meanwhile 200 mL·min^{-1} was the total flow rate of the feeding gas. Finally, the spectra were collected with subtraction from the background spectrum.

2.3. Activity measurements

NH_3-SCR of NO activity of all synthesized catalyst was carried out in a fixed-bed quartz tubular flow reactor in a steady state flow mode. The internal diameter of fixed-bed quartz tubular flow reactor was 6 mm. In the NH_3-SCR activity test, 0.400 g catalyst (40-60 meshes) was used. The composition of the feed gas was 1000 ppm NO, 1000 ppm NH_3, 3 vol% O_2, 6-12 vol% H_2O (when used), 100-200 ppm SO_2 (when used)

and N_2 as the balance gas, and gas hourly space velocity (GHSV) was 35,000-10,5000 h^{-1}. The NH_3-SCR experiments were operated in the temperature window of 20-420 °C. At each temperature, when the reaction got to a stable state (at least 40 min), the corresponding data were collected. Using the following equations, the NO conversion, NH_3 conversion and N_2 selectivity of the catalyst were calculated [10,27].

$$\text{NO conversion (\%)} = \frac{[NO]_{in} - [NO]_{out}}{[NO]_{in}} \times 100 \quad (1)$$

$$NH_3 \text{ conversion (\%)} = \frac{[NH_3]_{in} - [NH_3]_{out}}{[NH_3]_{in}} \times 100 \quad (2)$$

$$N_2 \text{ selectivity (\%)} = \frac{[NO]_{in} + [NH_3]_{in} - [NO_2]_{out} - 2[N_2O]_{out}}{[NO]_{in} + [NH_3]_{in}} \times 100 \quad (3)$$

In the above equations, $[NO]_{in}$ and $[NH_3]_{in}$ represent the NO and NH_3 inlet concentrations, respectively; and $[NO]_{out}$, $[NH_3]_{out}$, $[NO_2]_{out}$ and $[N_2O]_{out}$ denote the reactor NO, NH_3, NO_2 and N_2O outlet concentrations, respectively.

The relative turnover frequency (TOF) (moles number of NO converted by per molar surface copper per second / S^{-1}) of the catalyst was calculated according to the below Eq. (4) [33]. Where P is 101 KPa, V is the flow rate of NO (0.2 mL min^{-1}), R is 8.314 $J{\cdot}mol^{-1}{\cdot}K^{-1}$, α is the NO conversion (%), m_{cat} is the mass of catalyst (0.400 g), M_{cat} is the molar mass of the catalyst calculated from the XRF results, X_{cu} is the number of mol of cupper present in the catalyst, D is the dispersion of Cu (calculated according to the equations reported by Van Der Grift et al. [34]). The TOF value of each catalyst was calculated at 120, 150, 180 and 210 °C, respectively.

$$TOF = \frac{(Pv/RT)\propto}{X_{Cu}(m_{cat}/M_{Cat})D} \quad (4)$$

3. Results and discussion

3.1. Catalytic activity for NH_3-SCR

As displayed in Fig. 1(A), the CuO, Nb_2O_5 and Cu_x-$Nb_{1.1-x}$ (x = 0.45, 0.35, 0.25, 0.15) catalysts were examined for the NO conversion in the temperature range of 120 °C to 420 °C. Pure Nb_2O_5 showed almost no activity and CuO presented 90% activity at 250 °C. Nevertheless, the Cu_x-$Nb_{1.1-x}$ (x = 0.45, 0.35, 0.25, 0.15) catalysts exhibited 100% NO conversion in the temperature window of 210-300 °C. It was worth noting that the NO conversion was the first to increase and then decrease with the increase of copper amount below 210 °C. The NO conversion was 62%, 98%, 89% and 78% for $Cu_{0.15}$-$Nb_{0.95}$, $Cu_{0.25}$-$Nb_{0.85}$, $Cu_{0.35}$-$Nb_{0.75}$ and $Cu_{0.45}$-$Nb_{0.65}$, respectively at 180 °C. Among these catalysts, $Cu_{0.25}$-$Nb_{0.85}$ exhibited excellent low temperature activity with wide activity window of 170-370 °C (> 90% NO conversion).

The N_2 selectivity over CuO, Nb_2O_5 and Cu_x-$Nb_{1.1-x}$ (x = 0.45, 0.35, 0.25, 0.15) catalysts is given in Fig. 1(B). The Nb_2O_5 and CuO displayed the much lower N_2 selectivity which proceeding to decline at about 300 °C. For Cu_x-$Nb_{1.1-x}$ (x = 0.45, 0.35, 0.25, 0.15), the observed N_2 selectivity during the whole reaction temperature window was quiet significant. The N_2 selectivity was more than 95% over the $Cu_{0.15}$-$Nb_{0.95}$ catalyst, on other hand $Cu_{0.25}$-$Nb_{0.85}$, $Cu_{0.35}$-$Nb_{0.75}$ and $Cu_{0.45}$-$Nb_{0.65}$ displayed 100% N_2 selectivity.

The NH_3 conversion over the CuO, Nb_2O_5 and Cu_x-$Nb_{1.1-x}$ (x = 0.45, 0.35, 0.25, 0.15) catalysts during SCR reaction is displayed in Fig. 1(C). In the SCR reaction below 330 °C, the NH_3 conversion and analogous NO conversion was alike over each catalyst, demonstrating that both species were utilized with the equal molar ratio. While at above 330 °C, 100% NH_3 conversion over CuO and Cu_x-$Nb_{1.1-x}$ (x = 0.45, 0.35, 0.25, 0.15) catalysts was observed. The 100% NH_3 conversion is related to the over oxidation of NH_3 in addition to SCR reaction [27].

In catalyst design, the effect GHSV on NO conversion is considered to be a very important parameter [35]. In the series of our synthesized catalysts, the $Cu_{0.25}$-$Nb_{0.85}$ catalyst presented outstanding NO conversion and N_2 selectivity. Therefore, the $Cu_{0.25}$-$Nb_{0.85}$ catalyst was chosen to thoroughly explore the NH_3-SCR activity at different GHSV.

As shown in Fig. 1(D), the NO conversion over the $Cu_{0.25}$-$Nb_{0.85}$ catalyst at 35,000 and 70,000 h^{-1} GHSV was nearly same. On further increasing the GHSV from 70, 000 h^{-1} to 105,000 h^{-1}, the NO conversion was slightly decrease below 210 °C. However, the conversion was still more than 90% from 210 °C to 360 °C under GHSV of 105,000 h^{-1}. Hence, it is concluded from these results that the $Cu_{0.25}$-$Nb_{0.85}$ catalyst is excellent choice for NO removal in a wide temperature window of 180-360 °C even when the GHSV is as high as 105,000 h^{-1}.

3.2. H_2O and SO_2 stability

In the NH_3-SCR reaction, the SO_2 and water vapor are considered as main deactivating species [10,18,27]. For that reason, excellent SO_2 and H_2O durability of catalyst is required for NH_3-SCR. Among the series of our synthesized catalysts, the $Cu_{0.25}$-$Nb_{0.85}$ catalyst was used to investigate the SO_2 and H_2O resistance based on its excellent NH_3-SCR activity and the results are show in Fig. 2 and Fig. S1 (Supplementary Information). As displayed in Fig. 2(A), the SO_2 and H_2O durability test was conducted at 200 °C under GHSV of 35,000 h^{-1} and the reaction was operated for 4 h before exposing to SO_2. When 100 ppm SO_2 was introduced into the feed for 8 h, the NO conversion was not influenced and remained 100%. The results reveal that the $Cu_{0.25}$-$Nb_{0.85}$ catalyst has tremendous SO_2 resistance, and it is very important property for industrial use of a catalyst. In next 8 h, the amount of SO_2 increased from 100 ppm to 200 ppm in the feed, consequently the NO conversion decreased from 100% to 94.5%. When the SO_2 supply was removed, the NO conversion recovered to 100%. Further increasing SO_2 concentration to 300 ppm for 8 h, the NO conversion decreased to 78% as depicted in Fig. S1(A), and it also recovered to almost 100% after the SO_2 supply was turned off. Hence, the results suggest that the active site of $Cu_{0.25}$-$Nb_{0.85}$ catalyst was not blocked by SO_2. As exhibited in Fig. 2(A), the addition of 6% H_2O in the feed gas without SO_2, the NO conversion decreased to 94%. And further increasing the H_2O amount from 6% to 12%, the NO conversion reduced to 88%. Meanwhile, when the H_2O supply was turned off, the NO conversion restored to 100%. The results indicate that the presence of water vapor can restrain to the SCR reaction in some extent, but the deactivation is reversible. To examine the combined effect of SO_2 and H_2O on the NH_3-SCR activity, both SO_2 (100 ppm) and H_2O (12%) were introduced into the feed. The corresponding NO conversion decreased to 88% after 8 h, and restored to almost 100% when the SO_2 (100 ppm) and H_2O (12%) supply was turned off, suggesting the deactivation is also reversible. Thus, it can be summarized that the $Cu_{0.25}$-$Nb_{0.85}$ catalyst still displays outstanding NH_3-SCR of NO performance even in the presence of SO_2 and H_2O. The $Cu_{0.25}$-$Nb_{0.85}$ catalyst was also exposed to both SO_2 (300 ppm) and 6% H_2O for 12 h (Fig. S1(B)). The results demonstrated that the NO conversion decreased to 82% in the first 2 h. With the passage of time, the conversion was further decrease to 75% and remains at steady condition even after 10 h. When SO_2 and water vapor was turned off, it was observed that the NO conversion restored to about 100% and remained at this stable level. The results point out that the deactivation under high concentration SO_2 (300 ppm) is more serious than that under 100 ppm SO_2, however, it is still reversible.

Furthermore, the effect of H_2O on the activity was also studied in the testing temperature range over the $Cu_{0.25}$-$Nb_{0.85}$ catalyst. As shown in the Fig. 2(B), when 5% H_2O was added in the feed gas at much higher GHSV (70,000 h^{-1}), the NO conversion slightly decreased both at low and high temperature compared to the reaction without water (Fig. 1(A)). It is noteworthy that the $Cu_{0.25}$-$Nb_{0.85}$ catalyst still

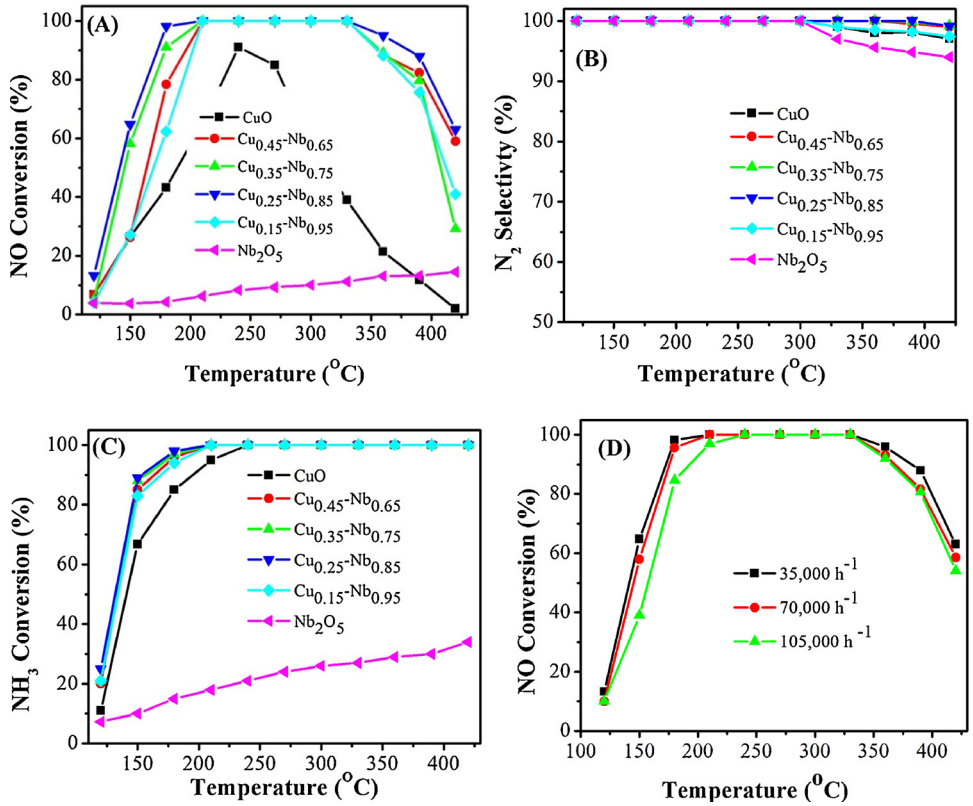

Fig. 1. (A) NO conversion, (B) NH_3 conversion (C) N_2 selectivity over Cu_x-$Nb_{1.1-x}$ (x = 0.45, 0.35, 0.25, 0.15) as a function of temperature, (D) Effect of GHSV on NO conversion over $Cu_{0.25}$-$Nb_{0.85}$ (Reaction conditions: [NO] = [NH_3] = 1000 ppm, [O_2] = 3% and N_2 balance).

displayed a broad temperature window of 185-380 °C at above 90% NO conversion even in the presence of 5% H_2O and under high GHSV of 70,000 h^{-1}. Thus, it can be concluded from the above results that $Cu_{0.25}$-$Nb_{0.85}$ can be considered as excellent catalyst for NH_3-SCR of NO.

Additionally, the H_2O resistance was performed at 180 °C under a GHSV of 35,000h^{-1} as depicted in Fig. S2. The SCR reaction was operated for 2 h before the addition of 6% H_2O. When 6% H_2O was added to the feeds, the NO conversion decreased to 90% in first 2 h, and then remained to 86% even after 10 h. The NO conversion recovered to almost 100% when the H_2O supply was turned off. These results indicate that the $Cu_{0.25}$-$Nb_{0.85}$ catalyst has also much higher water resistance at 180 °C.

3.3. Separated NO and NH_3 oxidation

To evaluate the redox ability of Cu_x-$Nb_{1.1-x}$ (x = 0.45, 0.35, 0.25, 0.15), the separated NO and NH_3 oxidation reaction were carried out over these catalysts. According to previous reports [11,36,37], if a catalyst during *in situ* NH_3-SCR conditions has the potential to fully oxidize NO to NO_2, then the deNO efficiency will be significantly increased at low temperature through "fast SCR" process (NO + NO_2 + $2NH_3 \rightarrow 2N_2 + 3H_2O$). As presented in Fig. S3(A), the NO_2 productions over the Cu_x-$Nb_{1.1-x}$ (x = 0.45, 0.35, 0.25, 0.15) catalysts were noticeably higher than that over Nb_2O_5 and CuO. Among the Cu_x-$Nb_{1.1-x}$ (x = 0.45, 0.35, 0.25, 0.15) catalysts, the $Cu_{0.25}$-$Nb_{0.85}$ catalyst displayed the best oxidation ability of NO to NO_2. Furthermore, the NO_2 production matched perfectly to the low-temperature NO conversion. These results demonstrate that mixing of Nb and Cu oxides together might efficiently enhance the NO oxidation in the process of NH_3-SCR process, and thus promote the NH_3-SCR performance.

The separated NH_3 oxidation results were depicted in Fig. S3(B). It can be observed that the conversion of NH_3 over the Cu_x-$Nb_{1.1-x}$ (x =

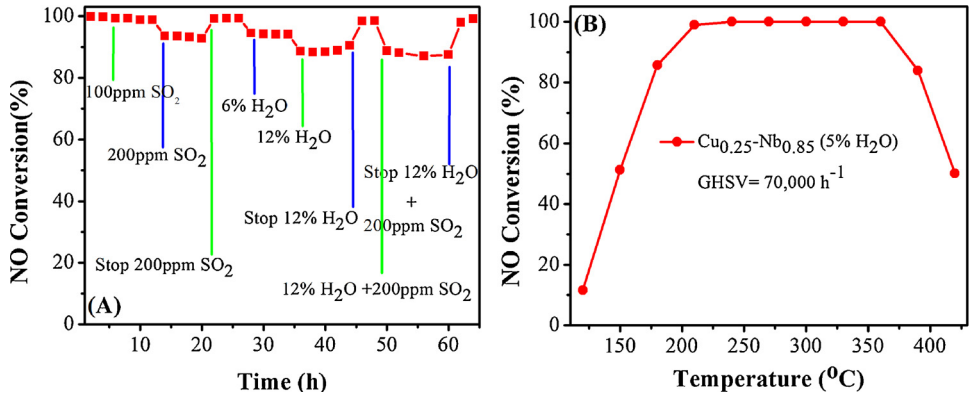

Fig. 2. Effect of SO_2, H_2O, and SO_2 + H_2O on NO conversion over $Cu_{0.25}$-$Nb_{0.85}$ at 200 °C under a GHSV of 35,000 h^{-1}, (B) Effect of 5% H_2O on NO conversion over $Cu_{0.25}$-$Nb_{0.85}$ at different temperature under a GHSV of 70,000h^{-1}.

Table 1
Physicochemical properties of Cu_x-$Nb_{1.1-x}$ (x = 0.45, 0.35, 0.25, 0.15) catalysts.

Samples	Cu/Nb atomic ratio [a]	S_{BET} [b] ($m^2\ g^{-1}$)	XPS data			H_2 consumption [f] ($\mu mol{\cdot}g^{-1}$)			Acid amount [g] ($\mu mol{\cdot}g^{-1}$)
			Cu^+/Cu [c] (%)	Nb^{5+}/Nb [d] (%)	O_α/O [e] (%)	α	β	α/(α+β)/%	
CuO	–	3	33.4	0	27.1	55.1	88.7	38.1	–
$Cu_{0.45}$-$Nb_{0.65}$	0.86	29	37.5	52.4	33.1	28.3	17.4	62.3	5.80
$Cu_{0.35}$-$Nb_{0.75}$	0.60	34	39.4	56.4	38.2	24.5	7.73	73.3	14.4
$Cu_{0.25}$-$Nb_{0.85}$	0.34	48	42.2	60.5	48.4	30.7	6.82	83.5	39.3
$Cu_{0.15}$-$Nb_{0.95}$	0.21	27	38.7	54.3	43.1	14.0	4.32	76.3	18.4
Nb_2O_5	–	17	0	47.4	25.4	0	0	0	–

[a] : the atomic ratio of Cu to Nb for the catalysts measured by XRF.
[b] : BET surface area.
[c] : the ratio of Cu^+ to (Cu^+ + Cu^{2+}).
[d] : the ratio of Nb^{5+} to (Nb^{5+} + Nb^{4+}).
[e] : the ratio of O_α to (O_α + O_β).
[f] : data calculated from H_2-TPR curves.
[g] : data calculated from NH_3-TPD curves.

0.45, 0.35, 0.25, 0.15) catalysts was much higher than that over Nb_2O_5 and CuO, which indicate that the NH_3 activation and redox property can be enhanced for the Cu_x-$Nb_{1.1-x}$ catalysts, and consequently it is useful for SCR process. Nevertheless, the NH_3 conversion was only 60% over Cu_x-$Nb_{1.1-x}$ (x = 0.45, 0.35, 0.25, 0.15) catalysts below 240 °C, which suggest the redox ability is mild that is favor of the high N_2 selectivity. Moreover, it is worth mentioning that the NH_3 conversion sharply increased with temperature and reached to 100% at 300 °C over Cu_x-$Nb_{1.1-x}$ (x = 0.45, 0.35, 0.25, 0.15). These results reveal that the decrease in the N_2 selectivity should be due to the over oxidation of NH_3 at high temperature (Fig. 1).

3.4. XRD and BET results

The elemental analysis was carried out through XRF. The atomic ratio of the Cu to Nb is 0.86, 0.60, 0.34 and 0.21 for $Cu_{0.45}$-$Nb_{0.65}$, $Cu_{0.35}$-$Nb_{0.75}$, $Cu_{0.25}$-$Nb_{0.85}$ and $Cu_{0.15}$-$Nb_{0.95}$ bimetal oxides catalysts, respectively (Table 1).

The XRD patterns of these catalysts are displayed in Fig. 3. It was found that the Cu_x-$Nb_{1.1-x}$ (x = 0.45, 0.35, 0.25, 0.15) catalysts showed very interesting XRD results. In the $Cu_{0.45}$-$Nb_{0.65}$ and $Cu_{0.35}$-$Nb_{0.75}$ catalysts, the diffraction peaks of CuO (PDF# 48-1548) were very weak [38], while the characteristic Nb_2O_5 phase (JCPDS 28-0317) was absent [9]. For $Cu_{0.15}$-$Nb_{0.95}$ catalyst, the observed weak diffraction peaks belonged to Nb_2O_5 phase. In the case of the $Cu_{0.25}$-$Nb_{0.85}$ catalyst, no diffraction peak was observed in Fig. 3. Only very weak peaks assigned to CuO and Nb_2O_5 appeared after the pattern was magnified to 6 times (Fig. S4). The above result indicate that strong interaction between Nb and Cu oxides does exist for the $Cu_{0.25}$-$Nb_{0.85}$ catalyst leading to the high dispersion of these oxides and consequently highly amorphous structure are formed [20,27]. The particle size was 23, 17 and 26 nm

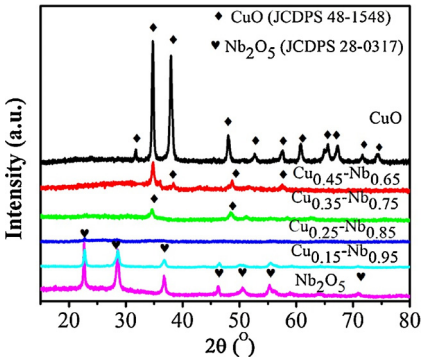

Fig. 3. XRD patterns of Cu_x-$Nb_{1.1-x}$ (x = 0.45, 0.35, 0.25, 0.15).

for $Cu_{0.15}$-$Nb_{0.95}$, $Cu_{0.35}$-$Nb_{0.75}$ and $Cu_{0.45}$-$Nb_{0.65}$, respectively, which was calculated by CuO (11-1) and Nb_2O_5 (001) crystal planes using Scherrer Equation. But the particle size of the $Cu_{0.25}$-$Nb_{0.85}$ catalyst can not be obtained using above method due to its nearly amorphous structure.

In Table 1 the BET surface areas of all synthesized samples were shown. The Cu_x-$Nb_{1.1-x}$ (x = 0.45, 0.35, 0.25, 0.15) catalysts demonstrated higher BET surface area than Nb_2O_5 and CuO. Furthermore, the $Cu_{0.25}$-$Nb_{0.85}$ catalyst offered the largest BET surface area (48 $m^2{\cdot}g^{-1}$), which consequently provide maximum active and adsorption sites, and thus up to some extent it contributed to the remarkable NH_3-SCR activity.

3.5. Raman spectra study

In Fig. S5, the Raman spectra of Nb_2O_5, CuO and Cu_x-$Nb_{1.1-x}$ (x = 0.45, 0.35, 0.25, 0.15) catalysts are depicted. The pure CuO sample displayed bands at 145, 290, 340, and 630 cm^{-1}, which can be attributed to the bulk CuO [39,40]. For pure Nb_2O_5 catalyst, four obvious bands were detected at 131, 231, 318, and 690 cm^{-1}, which can be ascribed to the Nb_2O_5 phase [32]. For the Cu_x-$Nb_{1.1-x}$ (x = 0.45, 0.35, 0.25, 0.15) catalysts, it was found that the peaks assigned to the Nb_2O_5 phase disappeared gradually with the increase in the ratio of Cu to Nb, meanwhile, the weak bands ascribed to the CuO phase were observed for $Cu_{0.35}$-$Nb_{0.75}$ and $Cu_{0.45}$-$Nb_{0.65}$. In case of $Cu_{0.25}$-$Nb_{0.85}$, hardly distinguishable bands for Nb_2O_5 phase were observed, while the CuO bands were completely absent. The above results illuminate that there is the strong interaction between Nb and Cu oxides in the Cu_x-$Nb_{1.1-x}$ (x = 0.45, 0.35, 0.25, 0.15) catalysts. Furthermore, the $Cu_{0.25}$-$Nb_{0.85}$ catalyst exhibits more clearly amorphous structure compared with $Cu_{0.15}$-$Nb_{0.95}$, $Cu_{0.35}$-$Nb_{0.75}$ and $Cu_{0.45}$-$Nb_{0.65}$, which strongly supports the XRD results.

3.6. TEM images

The TEM images in Fig. S6 showed that the $Cu_{0.15}$-$Nb_{0.95}$, $Cu_{0.25}$-$Nb_{0.85}$ and $Cu_{0.45}$-$Nb_{0.65}$ catalysts were assembled from small particles with about 20 nm in morphology which was in accord with the XRD results. The high-resolution TEM (HRTEM) images presented well resolved lattice fringes. The well-resolved periodic lattice fringe of 0.25 nm was consistent with the interplanar distance of the (11-1) plane of CuO phase. Similarly, a measured lattice spacing of 0.39 nm could be indexed to the (001) crystal plane of Nb_2O_5 phase. Furthermore, it is worth noting that each nanoparticle was attached to several other nanoparticles and no self-nucleated and isolated CuO or Nb_2O_5 nanoparticles were observed, and meanwhile the interface region was obviously observed between CuO and Nb_2O_5, indicating an intimate

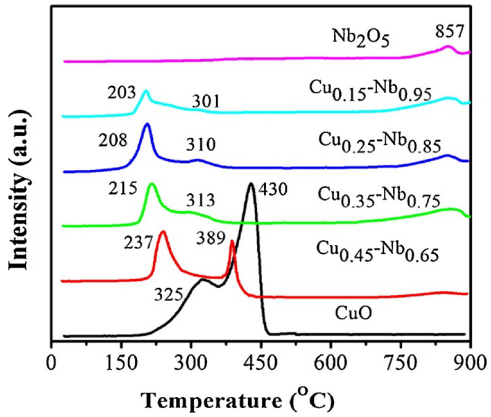

Fig. 4. H_2-TPR profiles of Cu_x-$Nb_{1.1-x}$ (x = 0.45, 0.35, 0.25, 0.15).

interfacial contact between the CuO and Nb_2O_5 nanoparticles. For $Cu_{0.25}$-$Nb_{0.85}$, the (11-1) plane of CuO phase and the (001) crystal plane of Nb_2O_5 phase were still observed after carefully searching in TEM images Fig. S6(B1) although it is almost amorphous structure that only very weak diffraction peak assigned to the CuO and Nb_2O_5 phase can be observed after the XRD pattern was magnified to 6 times.

3.7. H_2-TPR results

The reducibility of the chemical substance is widely analyzed through hydrogen temperature programmed reduction (H_2-TPR). The H_2-TPR results of these catalysts are displayed in Fig. 4. A single reduction peak appeared for pure Nb_2O_5 at 857 °C, which was allocated to the reduction of bulk niobium oxide [41,42]. For pure CuO, intense peak at 430 °C and a weak shoulder peak at 325 °C was observed that can be attributed to the bulk CuO and small size crystalline CuO, respectively. For the Cu_x-$Nb_{1.1-x}$ (x = 0.45, 0.35, 0.25, 0.15) catalysts, two separate peaks, intense peak at lower temperature (α peak) and the weak shoulder peak at higher temperature (β peak) were detected. The α peak located at 237, 215, 208 and 203 °C for $Cu_{0.45}$-$Nb_{0.65}$, $Cu_{0.35}$-$Nb_{0.75}$, $Cu_{0.25}$-$Nb_{0.85}$ and $Cu_{0.15}$-$Nb_{0.95}$, respectively, represented the reduction of highly disperse amorphous CuO particles (Cu^{2+}→Cu^{+1}→Cu°) [20,27]. While the β peak at 389, 313, 310 and 301 °C can be attributed to the reduction of minute crystalline CuO particles for $Cu_{0.45}$-$Nb_{0.65}$, $Cu_{0.35}$-$Nb_{0.75}$, $Cu_{0.25}$-$Nb_{0.85}$ and $Cu_{0.15}$-$Nb_{0.95}$, respectively [20,27,43]. It is noteworthy that increasing the Nb content and decreasing the Cu content in the samples lead to the shift of α peak to low temperature, indicating that the redox property increases with the decrease in the ratio of Cu to Nb for the Cu_x-$Nb_{1.1-x}$ (x = 0.45, 0.35, 0.25, 0.15) catalysts.

In addition, hydrogen consumption amount of the reduction peaks was calculated and the corresponding results were summarized in Table 1. The calculated hydrogen consumption ratio of α peak to (α + β) peak (α/(α + β)) for the Cu_x-$Nb_{1.1-x}$ (x = 0.45, 0.35, 0.25, 0.15) catalysts is over 60%, which indicate that less crystalline CuO and more highly dispersed CuO species were formed in the resultant catalysts. Among all catalysts, $Cu_{0.25}$-$Nb_{0.85}$ showed the maximum hydrogen consumption of the highly dispersed CuO (30.7 μmol·g^{-1}) and the largest hydrogen consumption ratio of α/(α + β) (83.5 %), although the Cu content is relative low. The above results are consistent with the XRD results. Therefore, it indicates that the $Cu_{0.25}$-$Nb_{0.85}$ sample contains less crystalline CuO species and more dispersed CuO species that presents much better redox property.

3.8. NH_3-TPD and NO-TPD analysis

The adsorption and activation of NH_3 on the surface active sites of catalyst plays a very important role in the NH_3-SCR reaction [11]. Therefore, NH_3-TPD of these catalysts was carried out to investigate their surface acid properties (Fig. 5(A)). For CuO and Nb_2O_5, no obvious desorption peak was observed. However, the Cu_x-$Nb_{1.1-x}$ (x = 0.45, 0.35, 0.25, 0.15) catalysts displayed two desorption peaks at low and high temperature. Based on the desorption peak area, the acid amounts of the Cu_x-$Nb_{1.1-x}$ (x = 0.45, 0.35, 0.25, 0.15) catalysts were calculated, and corresponding results were shown in Table 1. The acid amount is 5.80, 14.4, 39.3 and 18.4 μmol·g^{-1} for $Cu_{0.45}$-$Nb_{0.65}$, $Cu_{0.35}$-$Nb_{0.75}$, $Cu_{0.25}$-$Nb_{0.85}$ and $Cu_{0.15}$-$Nb_{0.95}$, respectively. Meanwhile, the $Cu_{0.25}$-$Nb_{0.85}$ catalyst possesses the most acidic sites (39 μmol·g^{-1}) among the Cu_x-$Nb_{1.1-x}$ (x = 0.45, 0.35, 0.25, 0.15) catalysts, it can contribute to the outstanding catalytic performance to some extent. The NH_3-TPD results indicate that the acidic amount increases obviously after mixing of Cu and Nb oxides, moreover, it is various with the ratio of Cu to Nb.

The NO-TPD results of Cu_x-$Nb_{1.1-x}$ (x = 0.45, 0.35, 0.25, 0.15) are displayed in Fig. 5(B). A single broad peak was observed for Nb_2O_5 at about 170 °C that belongs to the desorption of monodentate nitrate [13,27]. Two weak NO desorption peaks were observed in the range of 150-300 °C and 300-450 °C for CuO. Similarly, for Cu_x-$Nb_{1.1-x}$ (x = 0.45, 0.35, 0.25, 0.15) catalysts, the strong NO desorption peaks in the range of 150-300 °C and 300-450 °C can be attributed to the desorption of monodentate nitrate, bidentate nitrate and decomposition of bridging nitrates species, respectively [13,27]. It is noteworthy that the desorption peak area of the Cu_x-$Nb_{1.1-x}$ catalysts is much larger than that of CuO, suggesting far more amount of the NOx adsorbed sites on the Cu_x-$Nb_{1.1-x}$ catalysts. Among the Cu_x-$Nb_{1.1-x}$ (x = 0.45, 0.35, 0.25, 0.15) catalysts, $Cu_{0.25}$-$Nb_{0.85}$ showed the largest peak area especially at low temperature, pointing out the highest NO adsorption capacity.

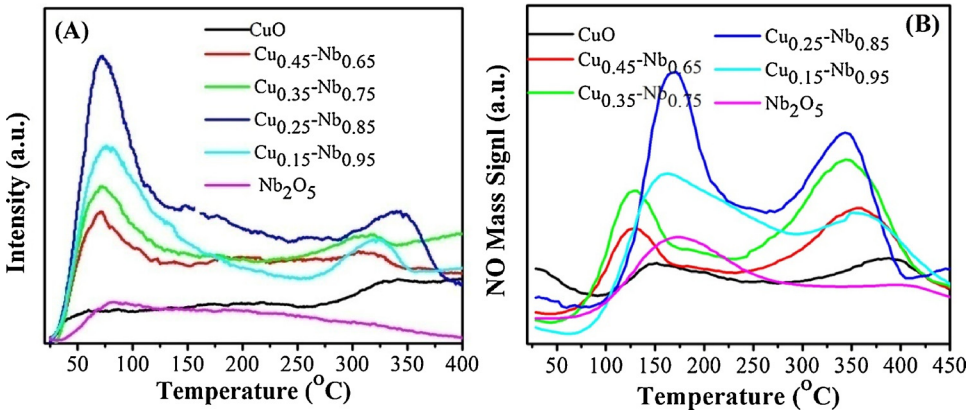

Fig. 5. (A) NH_3-TPD (B) NO-TPD curves of Cu_x-$Nb_{1.1-x}$ (x = 0.45, 0.35, 0.25, 0.15).

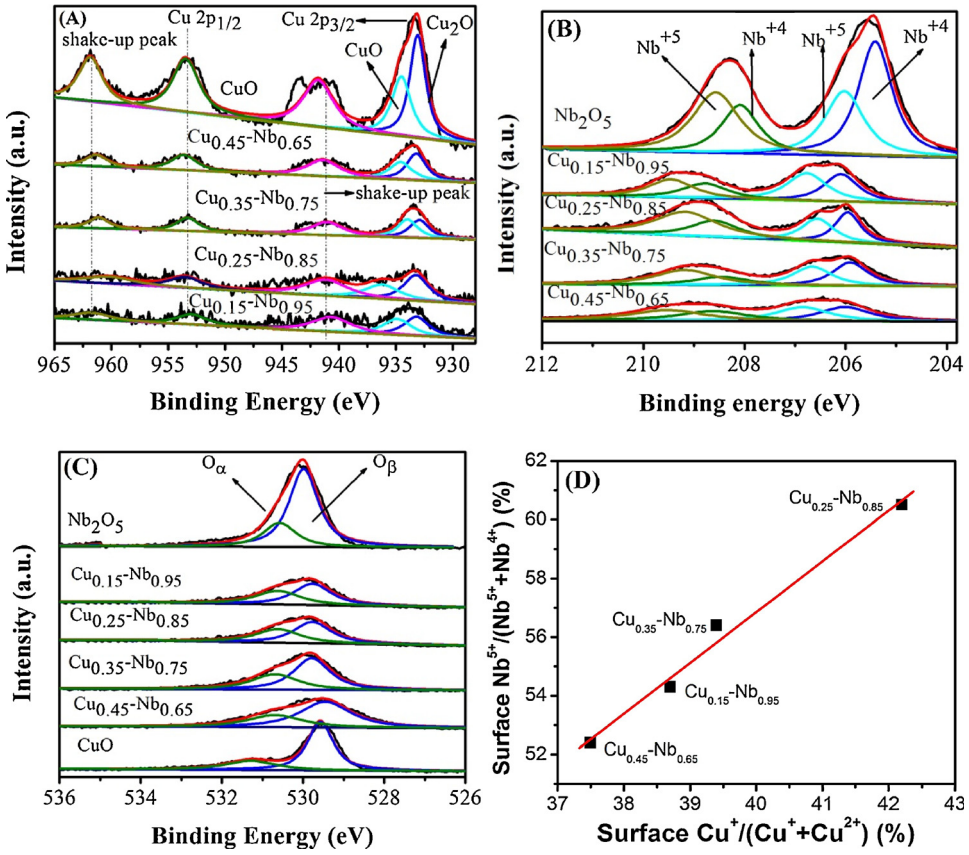

Fig. 6. XPS for (A) Cu 2p (B) Nb3d and (C) O1s, (D) relation between surface $Cu^{+}/(Cu^{+} + Cu^{2+})$ and $Nb^{5+}/(Nb^{5+} + Nb^{4+})$ of Cu_x-$Nb_{1.1-x}$ (x = 0.45, 0.35, 0.25, 0.15).

3.9. XPS study

The surface chemical states of copper, niobium and oxygen were investigated by XPS. In order to discriminate and understand the surface species, XPS of Cu2p, Nb3d and O1s were deconvoluted into numerous peaks by fitting Gaussian peaks after Shirley-background subtraction. Furthermore, the relative atomic concentration of different species was calculated from the area ratio of corresponding characteristic peaks, and their results are summarized in Table 1.

In the Fig. 6(A), the deconvoluted XPS of Cu2p for the Cu_x-$Nb_{1.1-x}$ catalysts are shown. The peaks detected at about 933.2 and 953.4 eV were assigned to $Cu2p_{3/2}$ and $Cu2p_{1/2}$. The presence of both Cu^{2+} and polycrystalline Cu_2O species in these samples was confirmed from the existence of shake up satellite peaks at 941.6 and 961.7 eV [44,45]. It can be concluded from these results that the Cu^{2+} and Cu^{+} species were coexistence on the surface of the Cu_x-$Nb_{1.1-x}$ (x = 0.45, 0.35, 0.25, 0.15) catalysts [46–48]. The corresponding relative percentage of the Cu species was calculated from the area ratio of Cu^{+} to $(Cu^{+} + Cu^{2+})$ $(Cu^{+}/(Cu^{+} + Cu^{2+}))$. As listed in Table 1, the $Cu_{0.25}$-$Nb_{0.85}$ catalyst displayed the highest amount of the Cu^{+} species (42.2%) among the Cu_x-$Nb_{1.1-x}$ (x = 0.45, 0.35, 0.25, 0.15) catalysts.

Nb3d spectra of Cu_x-$Nb_{1.1-x}$ (x = 0.45, 0.35, 0.25, 0.15) are presented in Fig. 6(B). According to previous reports [32,49,50], the binding energy of $Nb3d_{5/2}$ at about 206.1 and 205.3 eV could be attributed to the Nb^{5+} and Nb^{4+} species, respectively. For all synthesized catalysts, the corresponding relative percentage of the niobium species was calculated from the area ratio of Nb^{5+} to $(Nb^{5+} + Nb^{4+})$ $(Nb^{5+}/(Nb^{5+} + Nb^{4+}))$ listed in Table 1. The $Nb^{5+}/(Nb^{5+} + Nb^{4+})$ ratio was 54.3%, 60.5%, 56.4% and 52.4% for $Cu_{0.15}$-$Nb_{0.95}$, $Cu_{0.25}$-$Nb_{0.85}$, $Cu_{0.35}$-$Nb_{0.75}$ and $Cu_{0.45}$-$Nb_{0.65}$, respectively. The $Cu_{0.25}$-$Nb_{0.85}$ catalyst also showed the highest $Nb^{5+}/(Nb^{5+} + Nb^{4+})$ ratio among the Cu_x-$Nb_{1.1-x}$ (x = 0.45, 0.35, 0.25, 0.15) catalysts. Furthermore, compared with pure Nb_2O_5 sample, the binding energy of Cu_x-$Nb_{1.1-x}$ shifted to high value, implying that mixing of Cu and Nb oxides together altered the chemical environment around the Nb species [49,50]. As in the case of the $Cu_{0.25}$-$Nb_{0.85}$ catalyst, much less Cu^{2+} species are presented compared to $Cu_{0.45}$-$Nb_{0.65}$ and $Cu_{0.35}$-$Nb_{0.75}$, which interacts strongly with Nb^{4+} and prominent shift can be observed. While decreasing the Nb amount the interaction decreases between Cu and Nb, and consequently a slightly different shift is observed.

Combined the XPS results of Cu and Nb, it was found that there was a linear relation between surface $Cu^{+}/(Cu^{+} + Cu^{2+})$ and $Nb^{5+}/(Nb^{5+} + Nb^{4+})$ of Cu_x-$Nb_{1.1-x}$ (x = 0.45, 0.35, 0.25, 0.15) (Fig. 6(D)). Thus, it is suggested that the mixing of Cu and Nb oxides together probably can cause a redox reaction such as $Cu^{2+} + Nb^{4+} \leftrightarrow Cu^{+} + Nb^{5+}$, enhancing the redox ability of the Cu_x-$Nb_{1.1-x}$ catalysts. This is consistent with the results of H_2-TPR, separate NO and NH_3 oxidation.

As depicted in Fig. 6(C), the XPS spectra of O1s were fitted into two peaks. The O1s binding energy located at 530.4-531.1 eV was attributed to the chemisorbed oxygen species including O- and O_2- (donated as O_α) and the binding energy at 529.4.4-529.9 eV was ascribed to the lattice oxygen species (denoted as O_β) [51,52]. The relative concentration ratio of O_α to $(O_\alpha + O_\beta)$ $(O_\alpha/(O_\alpha + O_\beta))$ was summarized in Table 1. It was observed that the $(O_\alpha/O_\alpha + O_\beta)$ ratio of Cu_x-$Nb_{1.1-x}$ (x = 0.45, 0.35, 0.25, 0.15) was higher than that of CuO and Nb_2O_5. Moreover, the $Cu_{0.25}$-$Nb_{0.85}$ catalyst exhibited the highest $O_\alpha/(O_\alpha + O_\beta)$ ratio (48.4%) among Cu_x-$Nb_{1.1-x}$ (x = 0.45, 0.35, 0.25, 0.15). These results demonstrate that the $Cu_{0.25}$-$Nb_{0.85}$ catalyst possesses a large amount of the surface chemisorbed oxygen species, which is favor of NO oxidation to NO_2. It is in consistent with the oxidation of NO (Fig. S3(A)). Thus, the abundant amount of chemisorbed oxygen species on the surface of $Cu_{0.25}$-$Nb_{0.85}$ can lead to the quick NH_3-SCR reaction and consequently much better activity at low temperature (Fig. 1).

3.10. Interaction between Cu and Nb oxides

In the series of Cu_x-$Nb_{1.1-x}$ (x = 0.45, 0.35, 0.25, 0.15) catalysts, the complete NO conversion was observed for $Cu_{0.25}$-$Nb_{0.85}$ catalyst in a broad reaction temperature window of 180-330 °C, together with near 100% N_2 selectivity and remarkable SO_2/H_2O resistance. Furthermore, the $Cu_{0.25}$-$Nb_{0.85}$ catalyst can maintain the above performance even at very high GHSV of 105,000 h^{-1}, pointing out the developed SCR catalyst is a better choice for industrial use. However, it is noteworthy that TOF values (moles number of NO converted by per molar surface copper per second / S^{-1}) of the Cu_x-$Nb_{1.1-x}$ catalysts increase with the Cu amount in the catalysts at 120, 150, 180 and 210 °C (Fig. S10). The change of TOF values is not in agreement with the order of NO conversion at low temperature. The results indicate that the copper is not the only factor for NO conversion, and also confirm that the strong interaction between Cu and Nb oxides is responsible for the fascinating NO conversion results. The strong interaction between Cu and Nb oxides is addressed as follows.

The surface area, crystalline structure and surface redox property of the synthesized catalyst are greatly changed by the interaction between Cu and Nb oxides. The BET surface area of the Cu_x-$Nb_{1.1-x}$ (x = 0.45, 0.35, 0.25, 0.15) catalysts is higher than Nb_2O_5 and CuO, in which $Cu_{0.25}$-$Nb_{0.85}$ exhibited the highest BET surface area (48 $m^2\ g^{-1}$) that can make available more reaction sites, and subsequently contribute to the remarkable NH_3-SCR of NO activity to some extent. In the XRD patterns of Cu_x-$Nb_{1.1-x}$ (x = 0.45, 0.35, 0.25, 0.15), very weak diffraction peaks of CuO and Nb_2O_5 are observed. In the case of $Cu_{0.25}$-$Nb_{0.85}$ catalyst, almost no diffraction peak is observed, which implies that the corresponding metal oxides are highly dispersed and no formation of crystal structure of metal oxides. The Raman results (Fig. S5) are consistent with the XRD results. All the results of XRD, Raman and TEM images confirm the existence of strong interaction between Cu and Nb oxides in the Cu_x-$Nb_{1.1-x}$ (x = 0.45, 0.35, 0.25, 0.15) catalysts.

From H_2-TPR results (Fig. 4 and Table 1), the $Cu_{0.25}$-$Nb_{0.85}$ catalyst exhibits the highest α peak area and lowest β peak area in the series of Cu_x-$Nb_{1.1-x}$ (x = 0.45, 0.35, 0.25, 0.15) catalysts, suggesting the existence of more dispersed CuO species and less crystalline CuO species. It also indicates that the $Cu_{0.25}$-$Nb_{0.85}$ catalyst has excellent redox ability. The relative TOF value of NO confirms the NO conversion is closely related to the Cu species on the surface of the Cu_x-$Nb_{1.1-x}$ (x = 0.45, 0.35, 0.25, 0.15) catalysts (Fig. 7). The XPS results reveal that the strong interaction between Cu and Nb oxides probably leads to a redox reaction ($Cu^{2+} + Nb^{4+} \leftrightarrow Cu^{+} + Nb^{5+}$), and consequently enhancing the redox ability of the Cu_x-$Nb_{1.1-x}$ catalysts. This is consistent with the results of H_2-TPR, separate NO and NH_3 oxidation. Furthermore, the $Cu_{0.25}$-$Nb_{0.85}$ catalyst exhibited the highest $O_\alpha/(O_\alpha+O_\beta)$ ratio among the Cu_x-$Nb_{1.1-x}$ (x = 0.45, 0.35, 0.25, 0.15) catalysts. This result illustrates that the $Cu_{0.25}$-$Nb_{0.85}$ catalyst possesses a large amount of the surface chemisorbed oxygen species, which is favor of NO oxidation to NO_2 confirmed by the oxidation of NO (Fig. S3). Hence, the abundant amount of the surface chemisorbed oxygen species on $Cu_{0.25}$-$Nb_{0.85}$ can lead to the quick NH_3-SCR reaction and consequently much better activity at low temperature (Fig. 1).

The adsorption and activation of NH_3 on the surface active sites of catalyst play the key role in the NH_3-SCR reaction [11]. As shown in the NH_3-TPD (Fig. 5(A)), the acid amount of the Cu_x-$Nb_{1.1-x}$ (x = 0.45, 0.35, 0.25, 0.15) catalysts are obviously higher than pure CuO, and Nb_2O_5 because of the strong interaction between Nb and Cu oxides. Meanwhile, the $Cu_{0.25}$-$Nb_{0.85}$ catalyst possesses the most acidic sites (39.3 $\mu mol\cdot g^{-1}$) among the Cu_x-$Nb_{1.1-x}$ catalysts (Table 1), which may be responsible for its excellent SCR performance. In addition, the NO adsorption ability is also improved after the mixture of Cu and Nb oxides, meanwhile the $Cu_{0.25}$-$Nb_{0.85}$ catalyst presents the most NOx adsorbed sites from the NO-TPD results (Fig. 5(B)).

From the above discussion, the excellent SCR activity of the $Cu_{0.25}$-$Nb_{0.85}$ catalyst can be explained that on one hand the interaction of Nb and Cu oxides improves the redox property through the reaction ($Cu^{2+} + Nb^{4+} \leftrightarrow Cu^{+} + Nb^{5+}$), and as result increasing the chemisorbed oxygen species and charge imbalance. On the other hand, the interaction of Cu and Nb oxides also enhances the acidity and the NOx species adsorption on the surface of the $Cu_{0.25}$-$Nb_{0.85}$ catalyst, which is also significant for the NH_3-SCR of NO reaction.

In addition, the used $Cu_{0.25}$-$Nb_{0.85}$ catalyst after testing SCR activity according to the experimental condition in Fig. 1 was also characterized through XRD (Fig. S4), Raman (Fig. S7), H_2-TPR (Fig. S8), NH_3-TPD (Fig. S9), and XPS (Fig. S11) and the data are displayed in Table S1. The characterization results of the used $Cu_{0.25}$-$Nb_{0.85}$ catalyst were similar to those of the fresh $Cu_{0.25}$-$Nb_{0.85}$ catalyst, and no obvious change was observed. As presented in Fig. S12, the XPS results gave only 1.6% sulphur was tested on the surface of the used $Cu_{0.25}$-$Nb_{0.85}$ catalyst after SO_2 resistance, which demonstrate that the SO_2 did not deposit and block the active sites on the surface of catalyst. These results demonstrate that the structural and surface properties of the $Cu_{0.25}$-$Nb_{0.85}$ catalyst were not influenced during the SCR reaction.

3.11. In situ DRIFTS study

Based on the excellent SCR performance of the $Cu_{0.25}$-$Nb_{0.85}$ catalyst, *in situ* DRIFTS were carried out to investigate the surface adsorbed NOx and NH_3 species and their reactivity, furthermore to obtain the reaction process.

3.11.1. NH_3 or NO + O_2 adsorption ability

NH_3 adsorption on the $Cu_{0.25}$-$Nb_{0.85}$ catalyst with different interval of time was measured by *in situ* DRIFTS at 200, 150 and 100 °C, and the corresponding spectra are depicted in Fig. 7(A), Figs. S13 and S14,

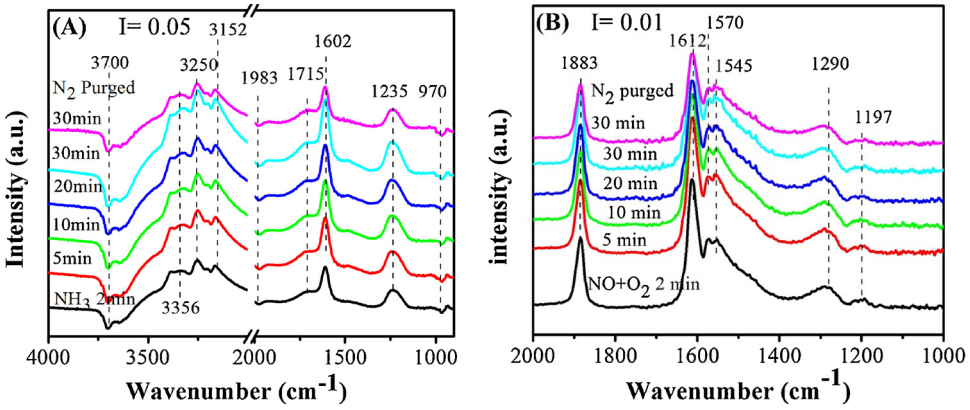

Fig. 7. DRIFTS of (A) NH_3 adsorption and (B) NO + O_2 adsorption on $Cu_{0.25}$-$Nb_{0.85}$ with different time at 200 °C.

respectively. It is noticed that the peak was saturated within 5, 10 and 10 min at 200, 150 and 100 °C, repectively. Several bands in the range of 1235-1715 cm^{-1} and 3100-3700 cm^{-1} were observed. The peaks at 1602 and 1235 cm^{-1} were ascribed to the symmetric and asymmetric vibration of NH_3 species adsorbed on Lewis acid sites, respectively [53–55]. The bands at 1715 cm^{-1} are attributed to the NH_4^+ formed on Brønsted acid sites [56]. The band centered around 3356, 3250 and 3152 cm^{-1} were attributed to the N-H stretching vibration [53]. The negative band observed at around 1983 cm^{-1} was ascribed to the Nb=O stretching mode, which reveals that during the NH_3 adsorption Nb=O were consumed [32]. But the negative band at about 970 cm^{-1} can not be observed due to the overlap of the noises at adsorption temperature of 100 and 150 °C [57]. During NH_3 adsorption the consumption of Nb-OH and Nb=O illustrate that both of Nb-OH [32] and Nb=O [57] could act as Brønsted and Lewis acid sites over $Cu_{0.25}$-$Nb_{0.8}$, respectively [32,57]. Furthermore, a negative band at 3652 cm^{-1} was detected, which was attributed to the consumption of surface O-H group [56,58]. So, the addition of niobium oxide species could increase Brønsted acidsites and Lewis acid sites, promoting the adsorption and activation of NH_3, which favored the SCR reaction [58].

To identify the reactivity of NH_3 species adsorbed on B and L acid sites on the $Cu_{0.25}$-$Nb_{0.85}$ catalyst under reaction condition, *in situ* DRIFT spectra were collected at temperature from 100 °C to 350 °C in a flow N_2 after NH_3 adsorption. In this experiment, initially the sample was purged with NH_3 for 1 h at 100 °C, and then purged with N_2 for 1 h. Finally, the spectrum was recorded and shown in Fig. 8. As mentioned above, several bands assigned to NH_4^+ formed on Brønsted acid sites and NH_3 species adsorbed on Lewis acid sites were observed. With the increase in temperature, the intensities of the bands belonging to the NH_4^+ adsorbed on Brønsted acid sites (1715 and 1453 cm^{-1}) decreased noticeably and completely disappeared at 250 °C, while the bands attributed to adsorbed NH_3 species on Lewis acid sites (1602 and 1235 cm^{-1}) still remained. The above results suggest that the NH_4^+ adsorbed on Brønsted acid sites exhibited less thermal stability and NH_3 species on Lewis acid sites had better thermal stability [57]. Therefore, the Brønsted acid sites might contribute to relatively lower temperature reaction and Lewis acid sites might contribute to both low and high temperature reaction [57]. In addition, the negative band at around 1983 cm^{-1} also became weaker and weaker with the increase in temperature, which further confirms Nb=O can be acidic sites.

The NO + O_2 adsorption on $Cu_{0.25}$-$Nb_{0.85}$ with time was carried out through *in situ* DRIFTS. As depicted in Fig. 7(B), several bands at 1883, 1612, 1570, 1545, 1290 and 1197 cm^{-1} were obtained. Two bands centered around 1570 and 1197 cm^{-1} were assigned to bidentate and bridged nitrate, and the bands located at 1545 and 1290 cm^{-1} were assigned to monodentate nitrates [58,59]. The strong band observed at 1612 cm^{-1} was ascribed to the absorbed NO_2 species [60,61], while the other strong band at 1883 cm^{-1} belonged to the adsorbed Cu^{2+}-NO (copper mononitrosyls) [20].

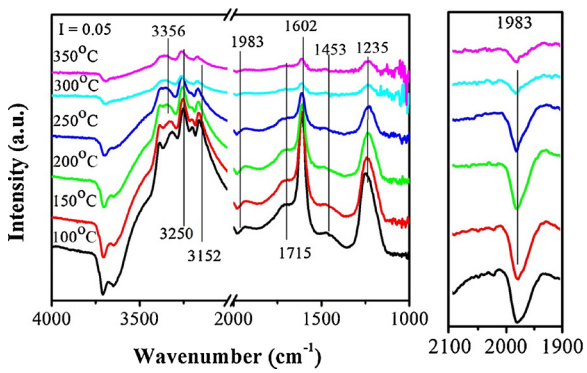

Fig. 8. DRIFTS of NH_3 adsorption and desorption at various temperatures over $Cu_{0.25}$-$Nb_{0.85}$.

The above results reveal that not only Brønsted acid and Lewis acid sites are present for NH_3 adsorption but also several NO*x* absorption sites are available on the surface of $Cu_{0.25}$-$Nb_{0.85}$. Furthermore, the niobium oxide species in the $Cu_{0.25}$-$Nb_{0.85}$ catalyst contributes to the enhancement of Lewis acid sites and Brønsted acid sites, and thus promoting the activation and adsorption of NH_3, which favors the NH_3-SCR of NO reaction [32,57].

3.11.2. Reaction between adsorbed NH_3 and NO + O_2 species

The reaction between adsorbed NH_3 and NO + O_2 species was recorded as function of time over $Cu_{0.25}$-$Nb_{0.85}$ at 200 °C and the corresponding spectra are displayed in Fig. 9(A). In this experiment, initially the sample was purged with NH_3 for 30 min and the spectrum was recorded, and then purged with N_2 for 30 min. In the final step, the catalyst was exposed to the NO + O_2 and the corresponding spectra were recorded as function of time. When the $Cu_{0.25}$-$Nb_{0.85}$ catalyst was exposed to NH_3 for 30 min, the symmetric and asymmetric vibration of NH_3 species adsorbed on Lewis acid sites (1610 and 1230 cm^{-1}) [53–55,62], NH_4^+ (1710 cm^{-1}) [56] and several peaks of N-H (3352, 3245 and 3155 cm^{-1}) [53–55,62] were detected. When NO + O_2 was introduced, all bands of the ammonia species disappeared after 5 min, with the appearance of new characteristic peaks were allocated to bridged nitrate and bidentate (1570 cm^{-1}, 1197 cm^{-1}) [53,55,62], monodentate nitrates (1545, 1282 cm^{-1}) [58,59], absorbed NO_2 species (1610 cm^{-1}) [60,61] and adsorbed copper mononitrosyls (Cu^{2+}-NO) [20]. Meanwhile, the intensity of these peaks increased with passage of time. It is concluded from the above results that the absorbed NH_3 species can react with the NO_x species and rapidly consumed after 2 min. Furthermore, it is also deduced that the symmetric and asymmetric vibration of NH_3 species adsorbed on Lewis acid sites and ionic NH_4^+ species bound to Brønsted acid site can participate in NH_3-SCR of NO.

3.11.3. Reaction between adsorbed NO + O_2 and NH_3 species

Reaction between adsorbed NO + O_2 and NH_3 species was performed over $Cu_{0.25}$-$Nb_{0.85}$ at 200 °C and the corresponding results are shown in Fig. 9(B). Initially, the sample was exposed to NO + O_2 gas, and then followed by N_2 purging for 30 min. Finally, NH_3 was added, and the corresponding spectra were collected at different time. As shown in Fig. 9(B), the bands of bidentate and bridged nitrate (1570 cm^{-1}, 1197 cm^{-1}) [53,55,62], monodentate nitrates (1545, 1282 cm^{-1}) [58,59], absorbed NO_2 species (1610 cm^{-1}) [60,61], and band of copper mononitrosyls (Cu^{2+}-NO) [20] were observed before NH_3 was added into the cell. After introducing NH_3 into the IR cell, the bands intensities of corresponding absorbed NO_2 species (1610 cm^{-1}) [60,61] and copper mononitrosyls (Cu^{2+}-NO) [20] decreased quickly and vanished after 2 min. While the band at 1545 cm^{-1} shifted to 1490 cm^{-1} which could be attributed to the deformation of the nitrate species [35]. After the consumption of the nitrate species, the characteristic coordinated NH_3 bands (1610 and 1230 cm^{-1}) [53–55,62], NH_4^+ (1710 cm^{-1}) [56], and several peaks of N-H (3352, 3245 and 3155 cm^{-1}) [53–55,62] were appeared. Hence, it is concluded from the above results that the absorbed NO_2 species (1610 cm^{-1}) [60,61], and bridged nitrate (1570 cm^{-1}, 1197 cm^{-1}) [53–55,62] are highly reactive at low temperature. On the other hand, the bands ascribed to bidentate nitrate (1570 cm^{-1}) [53,62], and the deform nitrate species (1490 cm^{-1}) [35] were detected even after 30 min, suggesting that these species were inactive during the reaction. Furthermore, the coexistence of NH_3 and adsorbed NO species on the surface of $Cu_{0.25}$-$Nb_{0.85}$ demonstrates that NH_3 and NO_x should adsorb on different active sites [52].

3.11.4. Co-adsorption of NO + O_2 + NH_3

To identify the species presented on the $Cu_{0.25}$-$Nb_{0.85}$ catalyst under reaction condition, *in situ* DRIFT spectra were collected at different temperature from 100 °C to 300 °C in a flow of NO + O_2 + NH_3. As displayed in Fig. 10, several bands were observed which were

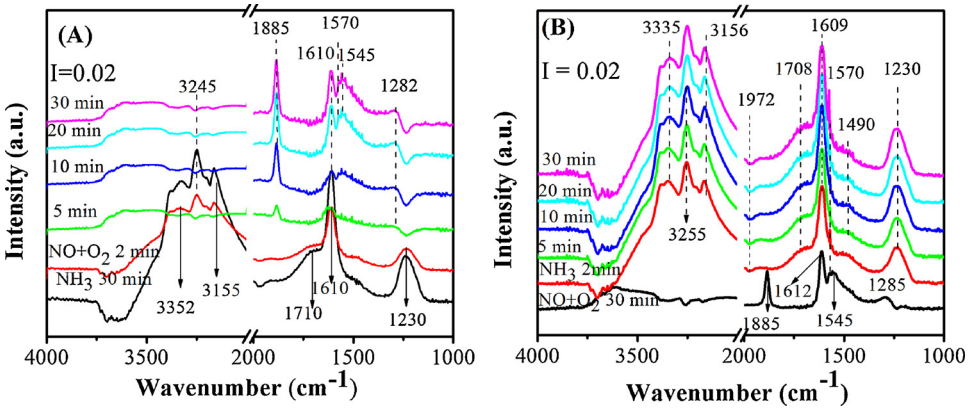

Fig. 9. (A) DRIFTS of NO + O_2 and pre-adsorbed NH_3 species at 200 °C on $Cu_{0.25}$-$Nb_{0.85}$ (Conditions: 1000 ppm NH_3 pre-absorbed followed by N_2 purging for 30 min, and then adding 1000 ppm NO + 5% O_2), (B) DRIFTS of NH_3 and pre-adsorbed NO_x species adsorbed species at 200 °C on $Cu_{0.25}$-$Nb_{0.85}$ (Condition: 1000 ppm NO + 5% O_2 pre-absorbed at 200°C followed by N_2 purging for 30 min, and then adding 1000 ppm NH_3).

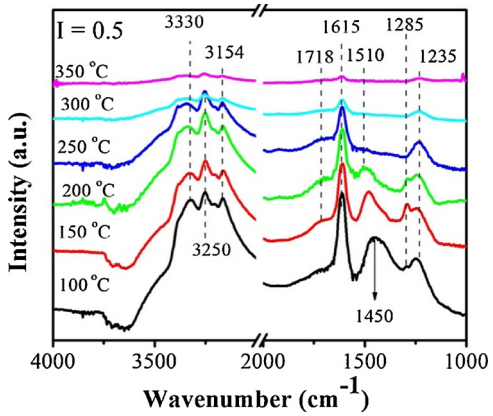

Fig. 10. DRIFTS of 1000 ppm NH_3 + 1000 ppm NO + 5% O_2 at various temperatures over $Cu_{0.25}$-$Nb_{0.85}$.

attributed to coordinated NH_3 on Lewis acid sites (3357, 3255, 3154 and 1235cm^{-1}) [53–55,62], the NH_4^+ adsorbed on Brønsted acid sites (1450 and 1715 cm^{-1}) [56], monodentate nitrates (1285 cm^{-1}) [58,59] at 100 °C, and the band at 1615 cm^{-1} might be due to the overlapping of bands of NH_3 and coordinated NO_2. The bands at 1495 and 1510 cm^{-1} could be attributed to the deformation of nitrate species at 150 and 200 °C, respectively [35]. With the increase in reaction temperature, the intensities of the bands belonging to the adsorbed NO_x species and NH_4^+ adsorbed on Brønsted acid sites decreased noticeably and completely disappeared at 250 °C, while the bands attributed to adsorbed NH_3 species on Lewis acid sites still remained. Combined with *in situ* DRIFTS results of NH_3 adsorption and desorption at different temperature (Fig. 8), it is concluded from the above results that both adsorbed NH_3 and NO_x species might be participated in the SCR reaction below 250 °C [32,57]. Moreover, the ionic NH_4^+ coordinated on the Bronsted acid sites are more reactive in low temperature (< 250 °C) as compared to NH_3 bonded to Lewis acid sites, while NH_3 bonded to Lewis acid sites are more reactive in high temperature (> 250 °C) [32,57].

According to pervious literatures [35,54,62], the Langmuir-Hinshelwood (L-H) at low temperature and Eley-Rideal (E-R) at high tetmperature are most commonly proposed reaction routes for the NH_3-SCR process. In addition, he adsorption of NH_3 has been considered as the beginning step for the NH_3-SCR reaction [63]. On the basis of our DRIFTS results, a simplified reaction process over the $Cu_{0.25}$-$Nb_{0.85}$ catalyst was proposed (Fig. S15). When the SCR reaction occurred below 250 °C, both adsorbed NO_x and NH_3 species were supposed to be participated in the NH_3-SCR process as displayed in the co-adsorption experiment of NH_3 + NO + O_2 (Fig. 10). From the experiment of "Reaction between adsorbed ammonia and species nitrogen oxides" (Fig. 9(A)), it is suggested that the coordinated NH_3 and the ionic NH_4^+ could participate in reaction with nitrate species. Moreover, in the SCR reaction the in situ formed NO_2 was generally considered to be a significant intermediate species [64,65], which was confirmed by the observation of the NO_2 species in Fig. 9(B). Therefore, below (< 250 °C), the in situ formed NO_2 specie, coordinated NH_3 and ionic NH_4^+ were regarded to be active species and involved in the NH_3-SCR process following an "L-H" route (Fig. S15).

When the SCR reaction occurred above 250 °C, the NH_3 adsorbed on Lewis acid sites became more active as shown in NH_3 + NO + O_2 co-adsorption experiment in Fig. 10. Bands at 1235 and 1615 cm^{-1} were ascribed to the σ_{as} and σ_s of NH_3 adsorbed on Lewis acid sites appeared and kept stable at below 250 °C. During the SCR reaction above 250 °C, this absorbed NH_3 first through oxidative dehydrogenation converted to NH_2 species, then reacts with NO to form unstable nitrosamine (NH_2NO) intermediate species [63, 66]. However, the band of NH_2NO species was not detected on the catalyst surface under the SCR condition due to its repaid decomposition into N_2 and H_2O [63, 66]. Thus, at high temperature (> 250 °C), the gas-phase or weakly adsorbed NO species react with NH_2 species following an E-R mechanism (Fig. S15).

4. Conclusion

A series of Cu_x-$Nb_{1.1-x}$ (x = 0.45, 0.35, 0.25, 0.15) oxides catalysts were prepared by a citric acid method and were applied in the NH_3-SCR process. The binary oxides catalysts (Cu_x-$Nb_{1.1-x}$ (x = 0.45, 0.35, 0.25, 0.15)) present 100% NO conversion in a broad reaction temperature window compared with single metal oxide catalysts such as CuO and Nb_2O_5. Among all the synthesized catalysts, the $Cu_{0.25}$-$Nb_{0.85}$ catalyst showed the complete NO conversion in a wide reaction temperature window from 180 °C to 330 °C, together with near 100% N_2 selectivity. The introduction of H_2O with SO_2 in the feeding gas has a reversible adverse influence on the NO conversion. The wide activity window of 185-380 °C can be maintained even in presence of 5% H_2O at high GHSV of 70,000 h^{-1} over $Cu_{0.25}$-$Nb_{0.85}$. The mixing of Nb and Cu together can cause a redox reaction such as Cu^{2+} + Nb^{4+} ↔ Cu^+ + Nb^{5+} leading to the excellent low temperature activity. Moreover, the $Cu_{0.25}$-$Nb_{0.85}$ catalyst has the most acid amount and NO adsorption capacity, which is responsible for has excellent NH_3-SCR activity.

Acknowledgements

This work is supported by Natural Sciences Fund of Heilongjiang Province (B2015009), Harbin science and technology innovation talent fund (Outstanding academic leader project) (RC2016XK015004), the Innovative Research Project of Key Laboratory of Functional Inorganic Material Chemistry (Heilongjiang University), Ministry of Education (2015).

Appendix A. Supplementary data

Supplementary material related to this article can be found, in the online version, at doi:https://doi.org/10.1016/j.apcatb.2018.05.014.

References

[1] M. Barreau, M.-L. Tarot, D. Duprez, X. Courtois, F. Can, Appl. Catal. B 220 (2018) 19.
[2] Z. Ma, X. Wu, H. Härelind, D. Weng, B. Wang, Z. Si, J. Mole. Catal. A 423 (2016) 172.
[3] T. Zhang, R. Qu, W. Su, J. Li, Appl. Catal. B 176 (2015) 338.
[4] M.F. Irfan, J.H. Goo, S.D. Kim, Appl. Catal. B 78 (2008) 267.
[5] J. Yu, Z. Si, M. Zhu, X. Wu, L. Chen, D. Weng, J. Zou, RSC Adv. 5 (2015) 83594.
[6] D. Nicosia, I. Czekaj, O. Kröcher, Appl. Catal. B 77 (2008) 228.
[7] Å. Kling, C. Andersson, Å. Myringer, D. Eskilsson, S.G. Järås, Appl. Catal. B 69 (2007) 240.
[8] S. Ding, F. Liu, X. Shi, H. He, Appl. Catal. B 180 (2016) 766.
[9] L. Chen, R. Li, Z. Li, F. Yuan, X. Niu, Y. Zhu, Catal. Sci. Technol. (2017).
[10] J. Li, H. Chang, L. Ma, J. Hao, R.T. Yang, Catal. Today 175 (2011) 147.
[11] G. Busca, L. Lietti, G. Ramis, F. Berti, Appl. Catal. B 18 (1998) 1.
[12] F. Liu, H. He, Y. Ding, C. Zhang, Appl. Catal. B 93 (2009) 194.
[13] J.P. Dunn, P.R. Koppula, H.G. Stenger, I.E. Wachs, Appl. Catal. B 19 (1998) 103.
[14] C. Tang, H. Zhang, L. Dong, Catal. Sci. Technol. 6 (2016) 1248.
[15] P. Li, Y. Xin, Q. Li, Z. Wang, Z. Zhang, L. Zheng, Appl. Catal. B 46 (2012) 9600.
[16] W. Xu, Y. Yu, C. Zhang, H. He, Catalysis Communications 9 (2008) 1453.
[17] M. Stanciulescu, G. Caravaggio, A. Dobri, J. Moir, R. Burich, J.-P. Charland, P. Bulsink, Appl. Catal. B 123 (2012) 229.
[18] Z. Si, D. Weng, X. Wu, J. Li, G. Li, J. Catal. 271 (2010) 43.
[19] L. Chen, Z. Si, X. Wu, D. Weng, ACS Appl. Mater. Interf. 6 (2014) 8134.
[20] J.H. Kwak, R.G. Tonkyn, D.H. Kim, J. Szanyi, C.H. Peden, J. Catal. 275 (2010) 187.
[21] T. Venkov, M. Dimitrov, K. Hadjiivanov, J. Mole, Catal. A 243 (2006) 8.
[22] M. Cortés-Jácome, C. Angeles-Chavez, E. Lopez-Salinas, J. Navarrete, P. Toribio, J. Toledo, Appl. Catal. A 318 (2007) 178.
[23] M.A. Cortés-Jácome, C. Angeles-Chavez, X. Bokhimi, J. Toledo-Antonio, J. Solid State Chem. 179 (2006) 2663.
[24] J.A. Sullivan, J.A. Doherty, Appl. Catal. B 55 (2005) 185.
[25] S. Suarez, J. Martin, M. Yates, P. Avila, J. Blanco, J. Catal. 229 (2005) 227.
[26] S. Ali, L. Chen, F. Yuan, R. Li, T. Zhang, X. Leng, X. Niu, Y. Zhu, Appl. Catal. B 210 (2017) 223.
[27] S. Okazaki, H. Kuroha, T. Okuyama, Chem. Lett. 14 (1985) 45.
[28] K. Vikulov, A. Andreini, E. Poels, A. Bliek, Catal. Lett. 25 (1994) 49.
[29] C. Petitto, H.P. Mutin, G. Delahay, Chem. Commun. 47 (2011) 10728.
[30] M. Casapu, O. Krocher, M. Mehring, M. Nachtegaal, C. Borca, M. Harfouche, D. Grolimund, J. Phys. Chem. C 114 (2010) 9791.
[31] R. Qu, X. Gao, K. Cen, J. Li, Appl. Catal. B 142 (2013) 290.
[32] G. Zhang, W. Han, H. Zhao, L. Zong, Z. Tang, Appl. Catal. B 226 (2018) 117.
[33] C.J.G. Van Der Grift, A.F.H. Wielers, B.P.J. Jogh, J. Van Beunum, M. De Boer, M. Versluijs-Helder, J.W. Geus, J. Catal. 131 (1991) 178.
[34] B. Guan, H. Lin, L. Zhu, Z. Huang, J. Phys. Chem. C 115 (2011) 12850.
[35] F. Liu, W. Shan, Z. Lian, L. Xie, W. Yang, H. He, Catal. Sci. Technol. 3 (2013) 2699.
[36] G. Qi, R.T. Yang, Appl. Catal. B 44 (2003) 217.
[37] T. Zhang, J. Liu, D. Wang, Z. Zhao, Y. Wei, K. Cheng, G. Jiang, A. Duan, Appl. Catal. B 148 (2014) 520.
[38] Z. Si, D. Weng, X. Wu, Y. Jiang, B. Wang, Catal. Sci. Technol. 1 (2011) 453.
[39] K.V. Chary, G.V. Sagar, D. Naresh, K.K. Seela, B. Sridhar, J. Phys. Chem. B 109 (2005) 9437.
[40] A.E. Lewandowska, M.A. Bañares, Catal. Today 118 (2006) 323.
[41] A. Sim, N.W. Cant, D.L. Trimm, Int. J. Hydrogen Energy 35 (2010) 8953.
[42] L. Xiaowei, S. Mingmin, H. Xi, Z. Haiyang, G. Fei, K. Yan, D. Lin, C. Yi, J. Phys. Chem. B 109 (2005) 3949.
[43] C.C. Chusuei, M. Brookshier, D. Goodman, Langmuir 15 (1999) 2806.
[44] S. Andonova, E. Vovk, J. Sjöblom, E. Ozensoy, L. Olsson, Appl. Catal. B 147 (2014) 251.
[45] T. Boningari, D.K. Pappas, P.R. Ettireddy, A. Kotrba, P.G. Smirniotis, Ind. Eng. Chem. Res. 54 (2015) 2261.
[46] F. Marquez, A. Palomares, F. Rey, A. Corma, J. Mater. Chem. 11 (2001) 1675.
[47] L. Martin, H. Martinez, D. Poinot, B. Pecquenard, F. Le Cras, J. Phys. Chem. C 117 (2013) 4421.
[48] A.M. Ruiz, G. Dezanneau, J. Arbiol, A. Cornet, J.R. Morante, Chem. Mater. 16 (2004) 862.
[49] D. Morris, Y. Dou, J. Rebane, C. Mitchell, R. Egdell, D. Law, A. Vittadini, M. Casarin, Phys. Rev. B 61 (2000) 13445.
[50] W. Shan, F. Liu, H. He, X. Shi, C. Zhang, Appl. Catal. B 115 (2012) 100.
[51] L. Chen, J. Li, M. Ge, J. Phys. Chem. C 113 (2009) 21177.
[52] M.A. Larrubia, G. Ramis, G. Busca, Appl. Catal. B 30 (2001) 101.
[53] M.A. Larrubia, G. Ramis, G. Busca, Appl. Catal. B 27 (2000) L145.
[54] G. Ramis, L. Yi, G. Busca, M. Turco, E. Kotur, R.J. Willey, J. Catal. 157 (1995) 523.
[55] J. Zawadzki, M. Wiśniewski, Carbon 41 (2003) 2257.
[56] Z. Lian, F. Liu, H. He, X. Shi, J. Mo, Z. Wu, Chem. Eng. J. 250 (2014) 390.
[57] D. Wang, L. Zhang, K. Kamasamudram, W.S. Epling, ACS Catal. 3 (2013) 871.
[58] S. Brandenberger, O. Kröcher, A. Wokaun, A. Tissler, R. Althoff, J. Catal. 268 (2009) 297.
[59] Y. Liu, T. Gu, X. Weng, Y. Wang, Z. Wu, H. Wang, J. Phys. Chem. C 116 (2012) 16582.
[60] Y.H. Yeom, B. Wen, W.M. Sachtler, E. Weitz, J. Phys. Chem. B 108 (2004) 5386.
[61] L. Chen, J. Li, M. Ge, Environ. Sci. Technol 44 (2010) 9590.
[62] Y. Shu, H. Sun, X. Quan, S. Chen, J. Phys. Chem. C 116 (2012) 25319.
[63] J.C. Dupin, D. Gonbeau, P. Vinatier, A. Levasseur, Phys. Chem. Chem. Phys. 2 (2000) 1319.
[64] X. Liu, K. Zhou, L. Wang, B. Wang, Y. Li, J. Am. Chem. Soc. 131 (2009) 3140.
[65] Z. Zhang, L. Chen, Z. Li, P. Li, F. Yuan, X. Niu, Y. Zhu, Catal. Sci. Technol. 6 (2016) 7151.